# Dual-Channel Flexible Strain Sensors Based on Mechanofluorescent and Conductive Hydrogel Laminates

Guoqing Lin, Muqing Si, Longgang Wang,* Shuxin Wei, Wei Lu,* Hao Liu, Yi Zhang, Danyang Li, and Tao Chen*

Flexible strain sensors are of great importance in many emerging applications for human motion monitoring, implanted devices, and human–machine interactive systems. However, the dual-channel sensing systems that enable both strain-dependent electronic and visually optical signal responses still remain underdeveloped, but such systems are of great interest for human–machine interactive uses. Here, inspired by the mechanically modulated skin color changes of squids via muscle contracting/releasing movements, a class of mechanofluorescent and conductive hydrogel laminates for visually flexible electronics is presented. The sensing laminates consist of interfacially bonded red fluorescent hydrogel, polydimethylsiloxane and carbon nanotubes (CNTs) film. Since the densely stacked microscopic CNTs film can be precisely stretched to induce the formation of network microcracks, the developed hydrogel laminates are endowed with simultaneous fluorescence-color and resistance changes, which can function as dual-channel flexible sensors for real-time human motion monitoring. These properties make the bioinspired soft hydrogel laminate electronics quite promising in the flexible electronics field.

## 1. Introduction

Flexible and stretchable electronic sensors are attracting increasing popularity in the applications as diverse as health monitoring, implanted devices, and human–machine interactive systems.[1–7] A large number of electronic strain sensors have been recently reported by integrating conductive fillers (such as carbon nanotubes, graphene, nanowires) into soft elastomer composites.[8–16] Nevertheless, most of these reported flexible strain sensors could only display one single electrical signal output, which might have some practical use limitations. Especially with the development of human–machine interactive systems, there has been an increasing demand for dual-channel reporting flexible sensors, which are capable of exhibiting both strain-dependent electrical and optical changes.[17–21] Among various optical means, fluorescence is believed to quite promising for wearable stretchable sensing uses because of its high sensitivity, fast response and operational simplicity. The most convenient strategy is to develop the mechanofluorescent elastomer materials with strain-dependent electrical signal response. One famous example was reported by Zhang and colleagues who draw inspiration from the muscle-controlled display tactics of cephalopods to present the robust nanostructured self-healable and mechanoluminescent elastomer composites, which were capable of displaying reversible strain-dependent luminescence and resistance response to tensile strain.[21]

Meanwhile, there has also been a growing interest to explore soft polymeric hydrogels for flexible sensors.[22–32] Different from elastomers, polymeric hydrogels usually have a 3D crosslinked hydrophilic network that is highly swollen by water.[5,33] Thus they are endowed with many unique advantages, including intrinsic soft wet nature, good biocompatibility, and especially tissue-like mechanical properties, which have made polymeric hydrogels promising candidates for flexible sensors.[34] In this context, considerable progresses have been recently achieved in soft conductive hydrogels with strain-dependent electronic signal changes. However, it still remains challenging to develop the promising dual-channel hydrogel systems with both sensitive conductivity and interactive fluorescence color changes to dynamic activities, which would show potentials to enable both electronic and visual monitoring of human motions. This is possibly because it is quite difficult to construct robust multifunctional materials with continuous and synergistic fluorescence/electronic signal responses over a wide strain range.

G. Lin, L. Wang
State Key Laboratory of Metastable Materials Science and Technology
Key Laboratory of Applied Chemistry
Hebei Key Laboratory of heavy metal deep-remediation in water and resource reuse
Yanshan University
Qinhuangdao 066004, China
E-mail: lgwang@ysu.edu.cn
G. Lin, M. Si, S. Wei, W. Lu, H. Liu, Y. Zhang, D. Li, T. Chen
Key Laboratory of Bio-Based Polymeric Materials Technology and Application of Zhejiang Province
Ningbo Institute of Material Technology and Engineering
Chinese Academy of Sciences
Ningbo 315201, China
E-mail: luwei@nimte.ac.cn; tao.chen@nimte.ac.cn
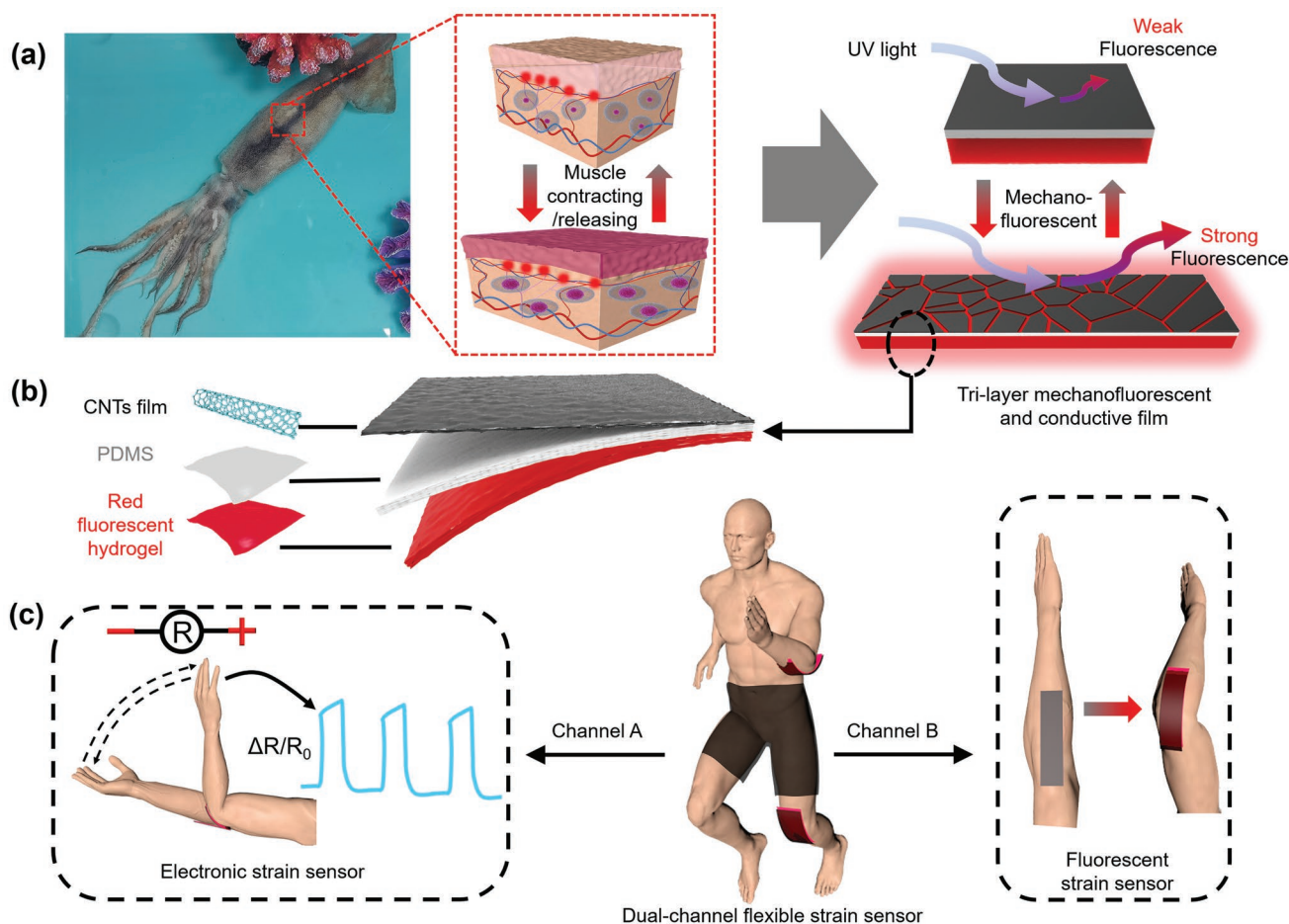
**Scheme 1.** a) Design of the bioinspired dual-channel flexible strain sensors based on mechanofluorescent and conductive hydrogel laminates. b) Illustration of the trilayer hydrogel laminate that was prepared by interfacial composition of red fluorescent hydrogel layer, PDMS and CNTs film. c) Schemes showing the dual-channel electronic and fluorescence color responses to human motions.

Herein, we draw inspiration from the mechanically modulated skin color changes of squids via muscle contracting/releasing movements[21,35–38] to develop a powerful kind of mechanofluorescent and conductive hydrogel laminates, which were capable of displaying dual-channel fluorescence color and electronic responses towards the strain changes. As illustrated in **Scheme 1**a,b, the flexible strain sensor consisted of three distinct material layers, that is, red fluorescent RB-PHEAA (Rhodamine B-functionalized poly(*N*-hydroxyethyl acrylamide)) hydrogel layer, polydimethylsiloxane (PDMS) thin film and densely stacked carbon nanotubes (CNTs) film. Such an interfacially composited structure is the key novelty of the present hydrogel laminate sensor, in contrast with most reported hydrogel strain sensors based on single-layer conductive polymeric hydrogel. Owing to this rational design, nearly no fluorescence was noticed from the CNTs film side by adhering the as-prepared trilayer film sensor onto the human skin (as illustrated in Scheme 1c), because the red fluorescence of the hydrogel layer was completely blocked by the tightly stacked CNTs film layer. Interestingly, upon human motions (e.g., elbow/knee bending), the tightly stacked CNTs film layer was stretched to induce the formation of microcracks, through which the red fluorescence was transmitted. Consequently,

increasing red fluorescence was observed with larger elbow/knee bending movements. Meanwhile, the electrically conductive path in the CNTs film layer was changed due to the formation of strain-induced microcracks, leading to simultaneous electrical signal change. In this way, the hydrogel-based dual-channel reporting flexible sensor that enabled both the electronic and optical detection of human motions was demonstrated.

## 2. Results and Discussion

### 2.1. Fabrication and Characterization of the Trilayer Fluorescent Hydrogel Laminates

**Figure 1**a and Figure S1 (Supporting Information) illustrate the procedure to prepare the trilayer mechanofluorescent hydrogel systems via the reported interfacial interpenetration strategy. Briefly, one PDMS thin film was first preloaded with the hydrophobic benzophenone (BP) initiator after being treated in the ethanol solution of BP at room temperature. Then, the BP-loaded PDMS film was used as the substrate to initiate the photopolymerization of aqueous solutions of *N*-(2-hydroxyethyl)acrylamide
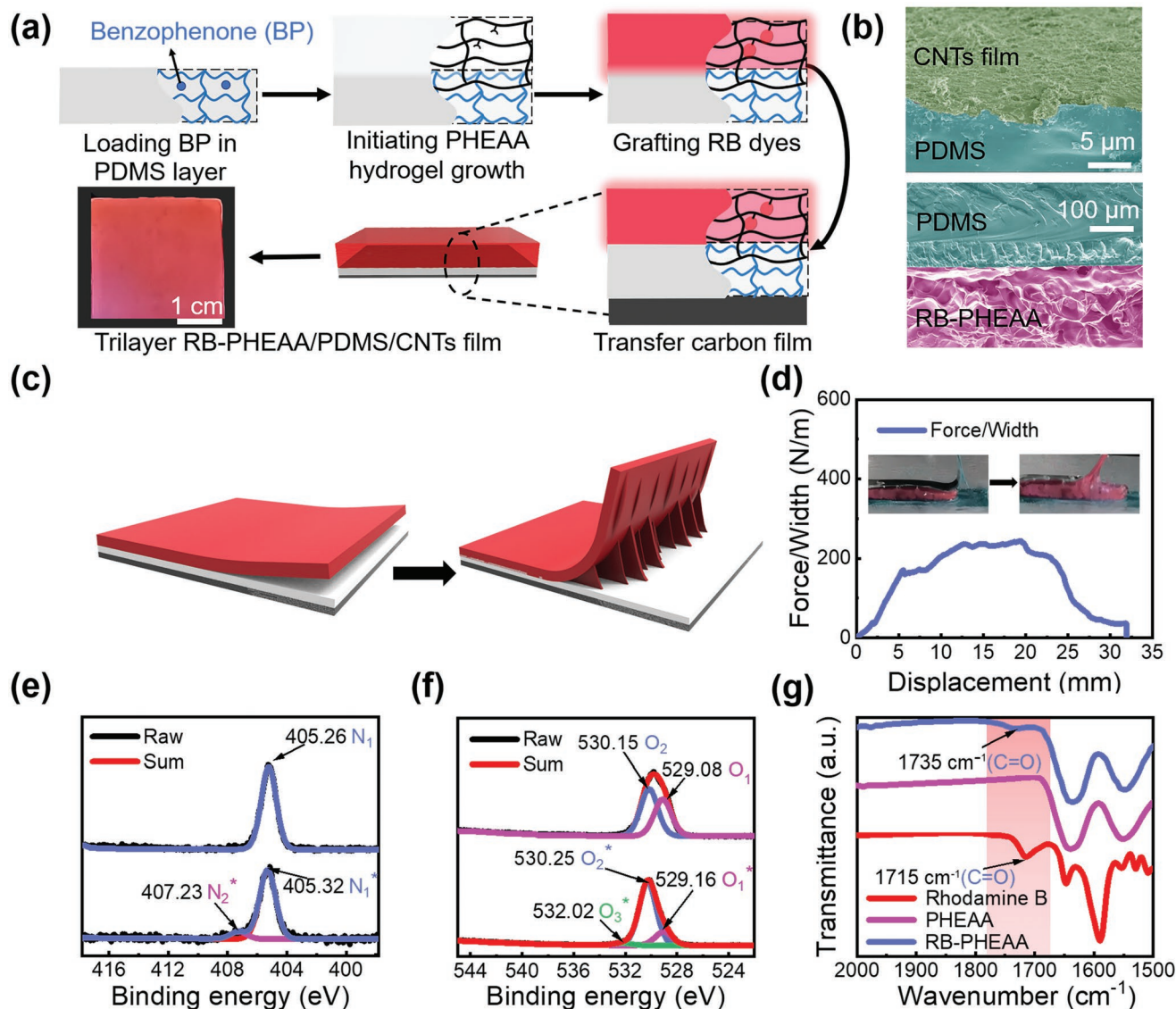
**ADVANCED
SCIENCE NEWS**

www.advancedsciencenews.com

**ADVANCED
OPTICAL
MATERIALS**

www.advopticalmat.de

**Figure 1.** a) The procedure to prepare the trilayer fluorescent hydrogel laminate, RB-PHEAA/PDMS/CNTs film. b) SEM images of the freeze-dried PHEAA/PDMS/CNTs film. c,d) Scheme of the peeling test, and curve of the peeling force per width of hydrogel sheet versus displacement. e–g) N 1s and O 1s spectra of the RB-PHEAA and PHEAA hydrogels, as well as their FT-IR spectrum.

(HEAA), 2-hydroxy-4″-(2-hydroxyethoxy)-2-methylpropiophenone (I-2959) and N,N″-methylenebisacrylamide (Bis), producing the bilayer PHEAA/PDMS film. To make the hydrogel layer fluorescent, the commercial Rhodamine B (RB) was covalently grafted onto the chemically crosslinked PHEAA network via an esterification reaction (Figure S2, Supporting Information).[39,40] After that, the densely stacked carbon nanotubes (CNTs) film, which was produced by the reported Marangoni spread[41,42] and capillary force induced compression of multiwall CNTs, was transferred onto the other side of the PDMS film.[43,44] Trilayer structure of the as-prepared RB-PHEAA/PDMS/CNTs film was clearly evidenced by the SEM images (Figure 1b), which shows that these three layers are bonded tightly. The peeling test demonstrated a large interfacial peeling force exceeding 250 N m$^{-1}$ per unit width between the fluorescent hydrogel layer and PDMS layer (Figure 1c,d).

To prove the covalent incorporation of Rhodamine B into the hydrogel layer, X-ray photoelectron spectra (XPS) and Fourier transform infrared spectrometer (FT-IR) spectral studies were conducted. As compared in Figure 1e,f, the XPS N 1s spectrum of the PHEAA hydrogel was fitted with only one component that can be assigned to the N atoms of the amide bond ($N_1$, 405.26 eV) (Figure S3, Supporting Information). While the N 1s spectrum of the RB-PHEAA hydrogel was deconvoluted into two peaks at 407.23 and 405.32 eV, which correspond to the amide bond on HEAA ($N_1^*$) and the N atoms of Rhodamine B ($N_2^*$) (Figure S3, Supporting Information). Similarly, the XPS O 1s spectrum of the PHEAA hydrogel was fitted with two components that can be assigned to the O atoms of the hydroxyl group ($O_1$, 529.08 eV) and carbonyl group ($O_2$, 530.15 eV) of HEAA (Figure S4, Supporting Information). The O 1s spectrum of the RB-PHEAA hydrogel

**ADVANCED
SCIENCE NEWS**
www.advancedsciencenews.com
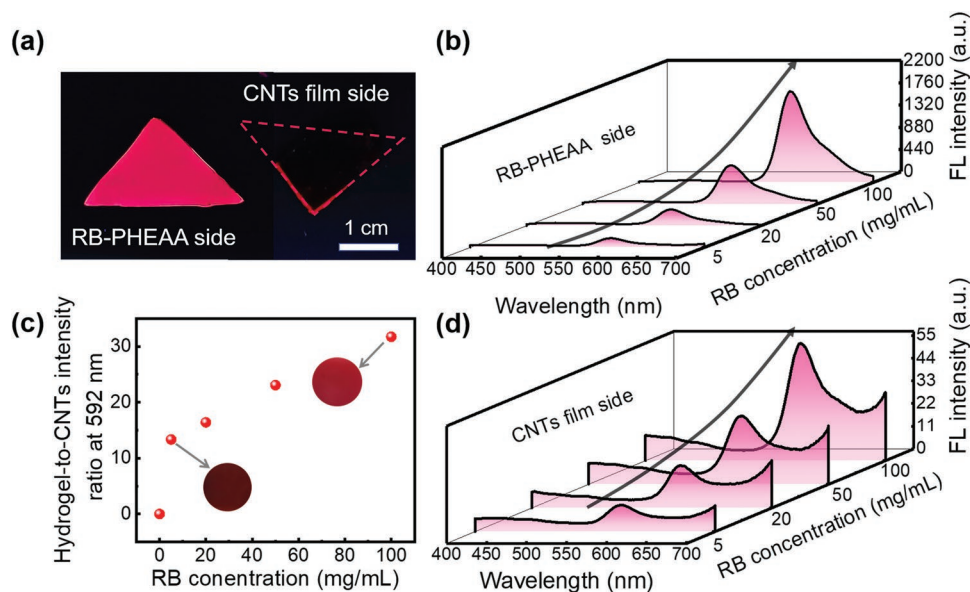
**ADVANCED
OPTICAL
MATERIALS**
www.advopticalmat.de

**Figure 2.** a) Photos of the RB-PHEAA/PDMS/CNTs film, which were taken from the RB-PHEAA hydrogel and CNTs film sides under a 365 nm UV lamp. b) The fluorescence spectra recorded from the RB-PHEAA hydrogel side. The films were prepared from the RB solutions with increasing concentration. c) The emission intensity ratio of the hydrogel-to-CNTs side at 592 nm. d) The fluorescence spectra recorded from the CNTs film side. Excitation at 365 nm for all fluorescent measurements.

was deconvoluted into three peaks at 529.16, 530.25, and 532.02 eV, which correspond to the O atom of free hydroxyl groups ($O_1^*$), the O atom of carbonyl oxygen ($O_2^*$), and the O atom of the ether group ($O_3^*$) (Figure S4, Supporting Information). In addition, Fourier Transform Infrared spectrometer (FT-IR) also proved that Rhodamine B was chemically grafted onto PHEAA. As shown in Figure 1g, the RB-PHEAA hydrogel shows noticeable characteristic peak at 1735 cm$^{-1}$, which are attributable to the C = O stretching vibrations of esters, while no such signal was observed for the PHEAA hydrogel. In addition, there was also no characteristic peak for the C = O stretching vibration of carboxylic acid in unmodified Rhodamine B at 1715 cm$^{-1}$ in the FT-IR spectrum of RB-PHEAA hydrogel. These results clearly indicated that Rhodamine B was chemically grafted onto PHEAA hydrogel and caused the stretching vibration frequency to shift from 1715 to 1735 cm$^{-1}$.

Fluorescent property of the as-prepared RB-PHEAA/PDMS/CNTs film was then studied. As shown in **Figure 2**a, its hydrogel side glowed intense red fluorescence under 365 nm UV light illumination, while the CNTs film side looked nearly nonfluorescent owing to the extremely low light transmittance of the densely stacked CNTs film layer. This observation was also evidenced by the recorded fluorescence spectra of both sides (Figure 2b–d). As expected, the fluorescence intensities of both sides could be significantly enhanced by increasing the grafting content of RB in the hydrogel layer. Moreover, the emission intensity ratio of the hydrogel-to-CNTs side could be raised up to ≈30 (Figure 2c), which was very helpful for the further mechanofluorescent studies. As detailed in Note S1 and Figure S5 (Supporting Information), the RB-PHEAA/PDMS/CNTs film prepared from 100 mg mL$^{-1}$ rhodamine B and 0.2 mm thickness PDMS was optimized to perform the best mechanofluorescent property.

## 2.2. Mechanofluorescent Studies

Since the developed hydrogel laminate sensor was primarily used as a strain sensor, the tensile properties of PDMS, PDMS/CNTs and RB-PHEAA/PDMS/CNTs films were tested and compared. As shown in Figure S6 (Supporting Information), RB-PHEAA/PDMS/CNTs film sensor can be easily stretched to more than 130%, suggesting its potential practical application for common human motion detection (<100% strain). **Figure 3**a depicts its mechanofluorescent photos that were taken from the CNTs side in response to external stretching stress. At the initiate state, nearly no fluorescence was observed owing to the excellent light-shielding capacity of the densely stacked CNTs film layer. When subject to stretching strain (e.g., 20%), the closely stacked structure of the CNTs film would be stretched to induce the formation of microcracks, which could be clearly observed on its laser confocal microscope image (Figure 3b). Consequently, a small bit of fluorescence light was transmitted through these micro-cracks to make the film weakly fluorescent. With the further increasing of stretching strain, more microcracks were produced, leading to the transmission of more fluorescence light. For example, when the strain was up to 100%, the emission intensity at 592 nm was enhanced by about 30-fold and thus intense red fluorescence was noticed (Figure 3c). Its strain-dependent fluorescence response was summarized and fitted in Figure 3d. It was found that the fluorescence intensity was in positive correlation with the external strain. When releasing the strain, the film spontaneously recovered to the initial non-fluorescent state, suggesting its desirable capacity for repetitive strain sensing via a mechanofluorescent visual response. It should be noted that there is no noticeable variation of the fluorescence emission of RB-doped hydrogel alone under different strains (Figures S7 and S8, Supporting Information). Even after several stretching-releasing cycles,
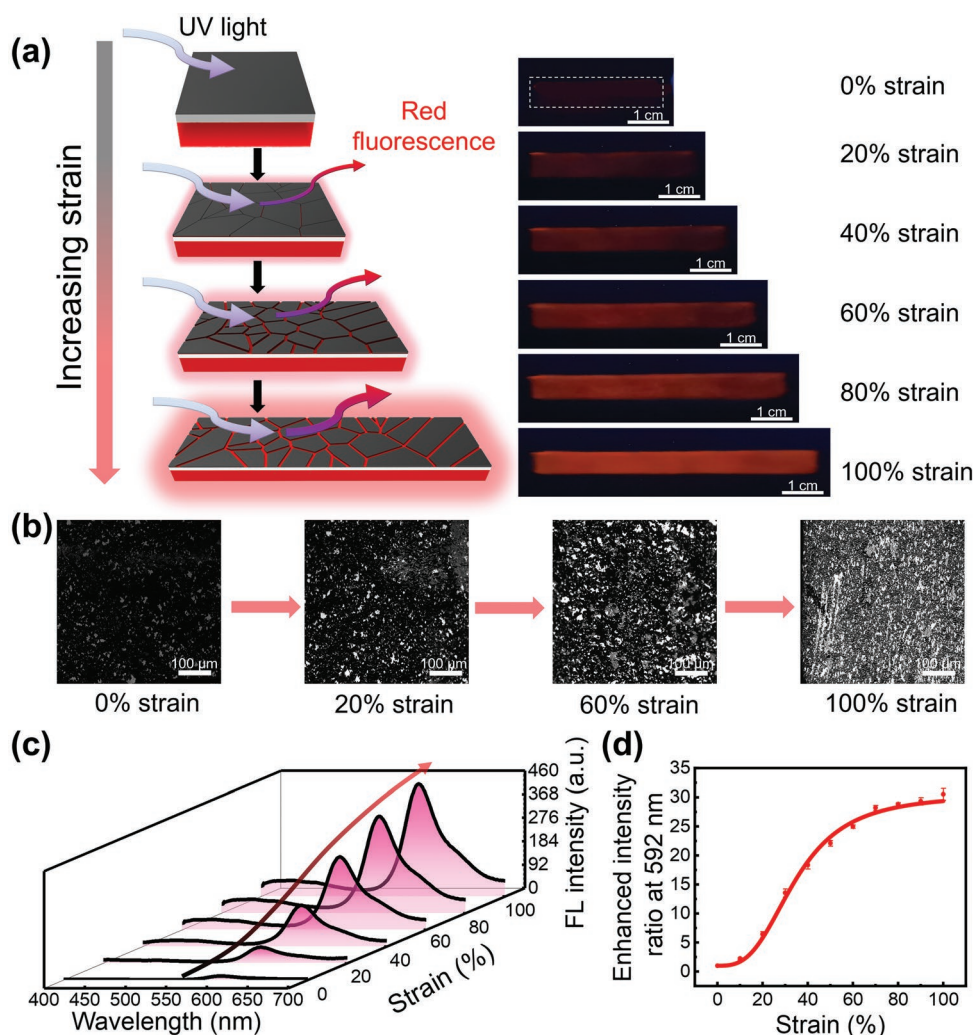
**ADVANCED
SCIENCE NEWS**

www.advancedsciencenews.com

**ADVANCED
OPTICAL
MATERIALS**

www.advopticalmat.de

**Figure 3.** a) Scheme and photos showing mechanofluorescent response of the RB-PHEAA/PDMS/CNTs film. b) Laser confocal microscope images showing the strain-induced formation of micro-cracks on the CNTs film side. c) Fluorescence spectra recorded from the CNTs film side under different strains. d) The curve showing the enhanced intensity ratio of CNTs film side at 592 nm versus strain.

its fluorescence intensity was still not changed significantly (Figure S9, Supporting Information). Moreover, the fluorescence intensities of RB-HEAA/PDMS under different strains were tested to check if the RB fluorescence intensity would be affected by the stretching-induced aggregation structure variation of PDMS. As shown in Figure S10 (Supporting Information), the fluorescence emission intensities of RB-HEAA/PDMS nearly keep constant under different strains, all these results clearly show the strain-dependent fluorescence response is indeed caused by the formation of microcracks in the CNTs film layer. Similarly, when the fluorescent hydrogel layer was functionalized with fluorescein, the strain-dependent green fluorescence intensity increment would be observed (Figure S11, Supporting Information), demonstrating the universal feature of the proposed mechanofluorescent hydrogel design.

To better showcase the mechanofluorescent property, its robust ability to display the colorful and meaningful fluorescent patterns was further demonstrated. To this end, additional patterned hydrogel layer with different-colored fluorescence was designed and covalently bonded with the red fluorescent RB-PHEAA hydrogel layer according to the reported method.[45,46] The preparation procedure was illustrated in **Figure 4**a. In a typical experiment, a blue fluorescent P(AAc-AAm-DAEAN) (PAAD) hydrogel was first produced by the radical polymerization of 4-(dimethylamino)ethoxy-*N*-allyl-1,8-naphthalimide (DAEAN), acrylic acid (AAc), acrylamide (AAm), potassium persulfate (KPS) and *N,N′*-methylenebisacrylamide crosslinker.[47] The blue fluorescent hydrogel was specially grafted with the active *N*-hydroxysuccinimide ester groups in order to enable the stable bonding between the P(AAc-AAm-DAEAN) and RB-PHEAA films via the esterification reaction depicted in Figure 4b,c. When these new devices were stretched by 50% under UV light, the hidden patterns ("CAS" or "10") were clearly revealed (Figure 4d). Releasing the strain would make these patterns hidden again. Such a capacity to enable the on–off switching of different fluorescent patterns is very interesting and expected to find potential uses for information decryption or on-demand display.[48,49]
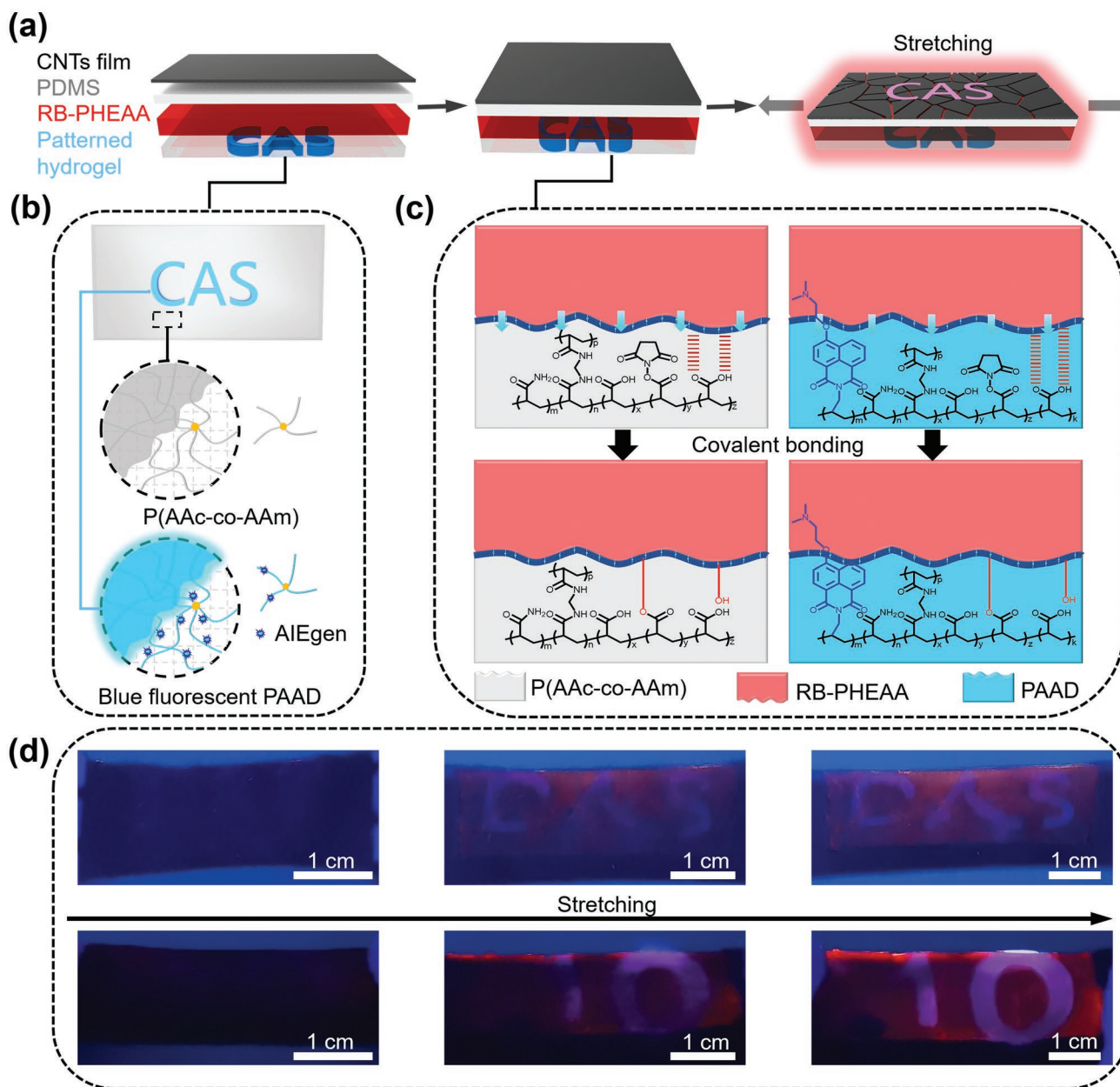
**Figure 4.** a) Scheme showing the preparation of the RB-PHEAA/PDMS/CNTs film with additional patterned hydrogel layer, as well as the strain-induced display of fluorescent pattern. b,c) Chemical structure of the additional patterned hydrogel layer, as well as the scheme showing its covalent bonding with RB-PHEAA hydrogel layer. d) Photos showing the strain-induced display of several fluorescent patterns.

## 2.3. Dual-Channel Sensor for Real-Time Human Motion Detection

Besides mechanofluorescent visual response, the strain-dependent resistance changes were also observed for the trilayer RB-PHEAA/PDMS/CNTs film. This is because the electrically conductive path in the CNTs film layer was gradually varied by the formation of microcracks. **Figure 5**a summarized its relative resistance changes ($\Delta R/R_0$) as a function of the stretching strain ($\varepsilon$), which were recorded according to the illustrated method.[13,50–52] For the convenience of quantitative description, Gauge factor

(GF = $(\Delta R/R_0)/\varepsilon$) was usually employed to evaluate the sensing performance of stretchable sensors. As fitted in Figure 5a, three distinct sensing ranges were noticed. At low strain (<20%), there is a slowly increasing relative resistance change with a small GF value ($\approx$7.7, the fitting correlation coefficient $R^2 = 0.997$). At medium strain range, $\Delta R/R_0$ rapidly increased with increasing stretching strain, producing a GF value as high as 29.9 with $R^2 = 0.997$. When further increasing the strain to 70% < $\varepsilon$ < 90%, the GF value declined again to 15.9 with $R^2 = 0.993$. Such good linearity of each sensing range is very appealing and beneficial for the accurate human motion detection.
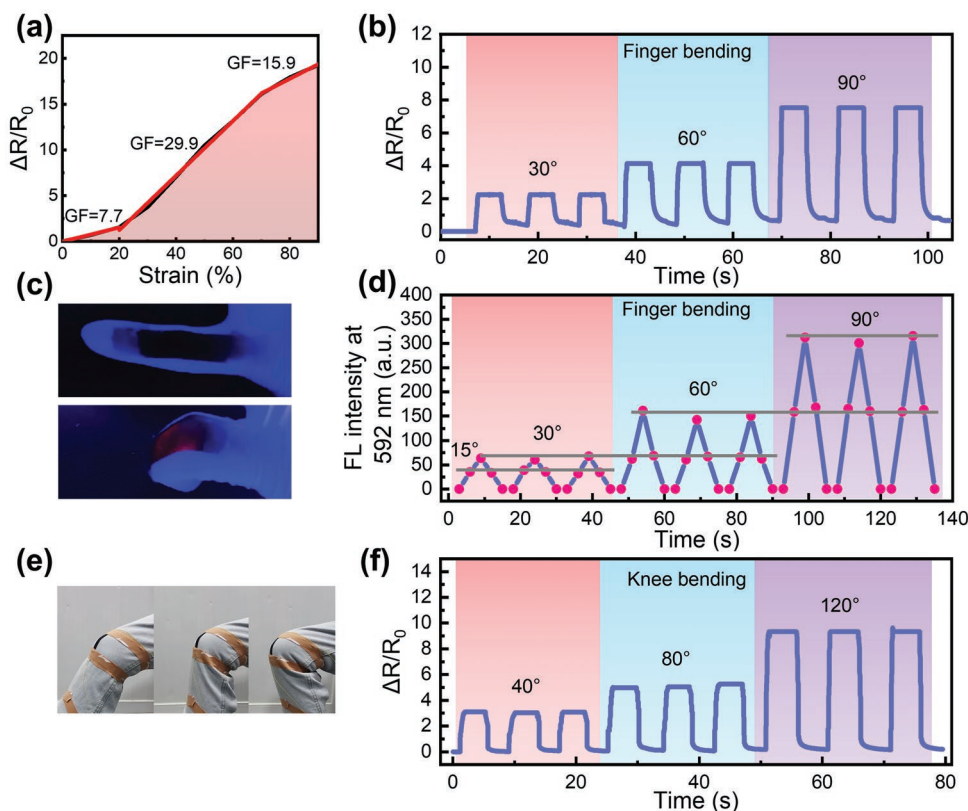
**Figure 5.** a) The curve showing the relationship between the resistance changes and strain. Gauge factor (GF = $(\Delta R/R_0)/\varepsilon$) was defined to evaluate the sensing performance of the RB-PHEAA/PDMS/CNTs film. b–d) The resistance and fluorescence intensity changes in response to different finger bending angles, as well as the photos showing the visual reporting of finger bending motion via fluorescence color change. e) Photos showing the method to detect the knee bending movement. f) The resistance changes in response to different knee bending angles.

Encouraged by the desirable strain-dependent visual and electrical responses of the RB-PHEAA/PDMS/CNTs device, we next tried to explore its potential use as the dual-channel flexible sensor for human motion detection. To do this, the film sensors were attached onto the finger, wrist, elbow and knee with the CNTs film side facing outward, which are schemed in Figures S12–S14 (Supporting Information). In the case of finger movement, when the finger bent against the film sensor, the nonfluorescent RB-PHEAA/PDMS/CNTs spontaneously became red fluorescent under UV light (Figure 5c). Meanwhile, real-time resistance changes were also observed. As recorded in Figure 5b, it was found that $\Delta R/R_0$ rose instantly as the finger quickly bent and stabilized when the finger remained at a certain angle. As expected, the resistance would fully recover to the initiate state when the finger was straightened again. Consistent results were recorded for several different tests, in which the finger was bent to the same angle. Importantly, upon increasing the finger bending angle, both larger resistance and fluorescence changes were recorded (Figure 5b,d), demonstrating the potential to report the finger motion through dual-channel electronic and optical signal responses. It should be noted that a prosthetic human hand was used to simulate the finger bending motion of a human finger and put into the fluorescence spectrometer in order to ensure the reproducibility of fluorescence sensing results (Figure S15, Supporting Information). Based on this method, fluorescence intensity changes of

the hydrogel laminate sensor could be accurately recorded by bending the prosthetic human hand finger to varying degrees. Besides finger motion, its capacity for the real-time detection of wrist, elbow, and knee movements was also demonstrated (Figure 5e,f and Figures S12–S14, Supporting Information). These results indicated that the flexible RB-PHEAA/PDMS/CNTs film exhibited both the noticeable fluorescence color-changing ability and electrical signal response to dynamic human body movements, suggesting its great potentials in visual human motion detection and human–machine interactive applications. Besides, the developed dual-channel flexible hydrogel sensor still shows consistent electrical signals after 500 stretching-releasing cycles (Figure S16, Supporting Information), indicating its satisfying sensing durability. All of these results imply that the developed flexible hydrogel strain sensor can not only inherit the soft wet nature and good biocompability, but also exhibit the desirable dual-channel reporting capabilities and satisfying sensing durability, compared with many previously reported strain sensors (Table S1, Supporting Information).

## 3. Conclusion

In summary, we have presented the design and fabrication of an efficient dual-channel flexible strain sensor that enabled both

**ADVANCED
SCIENCE NEWS**
www.advancedsciencenews.com

**ADVANCED
OPTICAL
MATERIALS**
www.advopticalmat.de

the electronic and visual detection of many important human joint motions. The sensing materials are prepared from the interfacial composition of red fluorescent hydrogel film, PDMS and conductive CNTs film. Owing to the soft wet nature and tissue-like mechanical features of the hydrogel layer, the as-prepared sensor can be conformably adhered onto the human skin with the CNTs film layer facing outwards. Under the human joint motions, the densely stacked CNTs film are stretched to induce the formation of micro-cracks, thus allowing both the fluorescence transmission of the hydrogel layer and conductive change of the CNTs film layer. Consequently, simultaneous fluorescent and electronic signal changes are measured to allow the real-time detection of human motions via the desirable dual-channel signal responses. In view of the modular design principle and facile operation, the proposed strategy is expected to be generally attractive and inspire the development of more powerful flexible electronics and devices.

## 4. Experimental Section

*Materials*: CNTs (OD 10–30 nm; length 10–30 μm; the COOH content 1.55%) with purity of over 90% were purchased from Chengdu Organic Chemistry Co. Ltd. *N*-(2-hydroxyethyl)acrylamide (HEAA, >98.0%), Rhodamine B (≥98.0%), acrylic acid (AAc, >99%), benzophenone (BP, 99%), 1-ethyl-3-(3-dimethylaminopropyl) carbodiimide hydrochloride (EDC·HCl, 98.0%), *N*,*N″*-methylenebisacrylamide (Bis, 99%), potassium persulfate (KPS, 99.99%), and fluorescein (90%) were purchased from Aladdin Chemistry Co. Ltd. Acrylic acid-*N*-succinimide ester (AAc-NHS-ester, 90%) and *N*-hydroxysuccinimide (NHS, 98%) were purchased from Energy Chemical. Polydimethylsiloxane (PDMS, 0.2–0.5 mm) were purchased from Xian Ruiya Organic Chemistry Co. Ltd. Acrylamide (AAM, 98.0%) and ethanol (99%) were obtained from Sinopharm Chemical Reagent Co. Ltd. 2-Hydroxy-4″-(2-hydroxyethoxy)-2-methylpropiophenone (I-2959, >98.0%) were purchased from TCI (Shanghai) Development Co. Ltd. 4-(2-dimethylaminoethyloxy)-*N*-allyl-1,8-naphthalimide (DAEAN) were synthesized according to the procedures described in the previous study.[47] HEAA passed through an alumina column to remove stabilizer before use. Other materials were used without further purification.

*Fabrication of the Bilayer RB-PHEAA/PDMS Film*: The PDMS elastomer (0.2–0.5 mm) was first immersed in an ethanol solution of benzophenone (10 wt%) for 8 h. The prepolymerization solution prepared by dissolving 1 g HEAA, 2 mg Bis and 10 mg I-2959 in 9 mL deionized water was added to the PDMS surface and then sealed in a self-made mold (the mold is a square, with a side length of 3 cm and a thickness of 0.5 mm). After being irradiated under a 15 W 365 nm UV light for 120 min, the bilayer PHEAA/PDMS film (PHEAA layer thickness ≈0.5 mm, PDMS layer thickness ≈0.2 mm) was obtained. To covalently graft Rhodamine B into the hydrogel layer, the as-prepared bilayer PHEAA/PDMS film was placed into the aqueous solutions of RB (5–100 mg mL$^{-1}$), EDC·HCl (2 mg mL), and NHS (1 mg mL$^{-1}$) at room temperature (20–35 °C) and then shaken for 48 h. After that, the bilayer RB-PHEAA/PDMS film was washed by a large amount of ethanol and deionized water in order to completely remove the unreacted RB molecules.

*Fabrication of the Trilayer RB-PHEAA/PDMS/CNTs Film*: The densely stacked CNTs film was prepared according to the previously reported method.[13,53] The as-prepared bilayer RB-PHEAA/PDMS film was first cut into the appropriate shape (a rectangle with the length of 3 cm and the width of 1 cm) and then conformally fixed on a PET substrate. Using the lift-up transferring method, the CNTs film floating on the air/water interface was facilely transferred to the PDMS side to obtain the trilayer RB-PHEAA/PDMS/CNTs film.

*Fabrication of the Patterned Hydrogel*: The blue fluorescent hydrogel was prepared by the thermal-induced radical polymerization of the prepolymerization solution of 0.9 mL AAc, 0.9 g AAm, 0.05 g DAEAN, 0.005 g Bis, 0.04 g AAc-NHS-ester, and 0.02 g KPS in 8 mL deionized water at 80 °C for 8 h. After that, the blue fluorescent hydrogel was cut into the required shape such as such as "CAS" and "10," which were then placed on a glass substrate and sealed with the hydrogel prepolymerization solution (without the blue fluorescent DAEAN monomer) at 80 °C for 8 h. Finally, the patterned hydrogel sample was obtained. (The patterned hydrogel is a rectangle with the length of 3 cm and the width of 1 cm, thickness of the hydrogel is 0.5 mm).

*Characterization*: Mechanofluorescent photos of the RB-PHEAA/PDMS/CNTs film were recorded by smart phone camera (Honor X10) under a UV lamp (ZF-5, 8 W, 365 nm). Steady-state fluorescence spectra were measured by Hitachi F-4600 fluorescence spectrofluorometer with a Xenon lamp (150 W). The morphology of the freeze-dried sample was characterized by a field-emission scanning electron microscope (SEM, Hitachi S-4800, 4 kV). Micro morphology of carbon film side was characterized by a biological laser scanning confocal microscopy (TCS SP5). The chemical structure of hydrogels were characterized by Fourier transform infrared spectrometer (NICOLET 6700) and X-ray photoelectron spectroscopy (AXIS SUPRA). The mechanical properties were characterized with a 1 kN universal stretching machine (Zwick/Roell Z1.0). Electronic sensing performance of RB-PHEAA/PDMS/CNTs film was tested by electrochemical work station (CH Instruments, CHI660E. Chenhua Co., Shanghai, China).

## Supporting Information

Supporting Information is available from the Wiley Online Library or from the author.

## Conflict of Interest

The authors declare no conflict of interest.

## Data Availability Statement

Research data are not shared.

[1] L. Hu, Y. Wan, Q. Zhang, M. J. Serpe, *Adv. Funct. Mater.* **2019**, *30*, 1903471.

**ADVANCED
SCIENCE NEWS**

www.advancedsciencenews.com

**ADVANCED
OPTICAL
MATERIALS**

www.advopticalmat.de

[2] L. Hu, Q. Zhang, X. Li, M. J. Serpe, *Mater. Horiz.* **2019**, *6*, 1774.

[3] Y. Jang, S. M. Kim, G. M. Spinks, S. J. Kim, *Adv. Mater.* **2020**, *32*, 1902670.

[4] Z. Li, P. Liu, X. Ji, J. Gong, Y. Hu, W. Wu, X. Wang, H. Q. Peng, R. T. K. Kwok, J. W. Y. Lam, J. Lu, B. Z. Tang, *Adv. Mater.* **2020**, *32*, 1906493.

[5] S. Wei, Z. Li, W. Lu, H. Liu, J. Zhang, T. Chen, B. Z. Tang, *Angew. Chem., Int. Ed.* **2021**, *60*, 8608.

[6] H. Yuk, B. Lu, X. Zhao, *Chem. Soc. Rev.* **2019**, *48*, 1642.

[7] Y. Zhang, H. Wang, H. Lu, S. Li, Y. Zhang, *Iscience* **2021**, *24*, 102716.

[8] S. Lin, X. Zhao, X. Jiang, A. Wu, H. Ding, Y. Zhong, J. Li, J. Pan, B. Liu, H. Zhu, *Small* **2019**, *15*, 1900848.

[9] H. Yan, M. Zhong, Z. Lv, P. Wan, *Small* **2017**, *13*, 1701697.

[10] Q. Y. Chen, H. Tang, J. L. Liu, R. R. Wang, J. Sun, J. R. Yao, Z. Z. Shao, X. Chen, *Chem. Eng. J.* **2021**, *422*, 130091.

[11] H. Wang, Y. Zhang, X. Liang, Y. Zhang, *ACS Nano* **2021**, *15*, 12497.

[12] W. Pu, D. Fu, Z. Wang, X. Gan, X. Lu, L. Yang, H. Xia, *Adv. Sci.* **2018**, *5*, 1800101.

[13] S. Wang, P. Xiao, Y. Liang, J. Zhang, Y. Huang, S. Wu, S. W. Kuo, T. Chen, *J. Mater. Chem. C* **2018**, *6*, 5140.

[14] X. Liang, H. Li, J. Dou, Q. Wang, W. He, C. Wang, D. Li, J. M. Lin, Y. Zhang, *Adv. Mater.* **2020**, *32*, 2000165.

[15] H. Wang, S. Li, Y. Wang, H. Wang, X. Shen, M. Zhang, H. Lu, M. He, Y. Zhang, *Adv. Mater.* **2020**, *32*, 1908214.

[16] K. Xia, K. Wu, M. Zhu, X. Shen, Z. Yin, H. Wang, S. Li, M. Zhang, H. Wang, H. Lu, A. Pan, C. Pan, Y. Zhang, *Sci. Bull.* **2020**, *65*, 343.

[17] S. Zeng, D. Zhang, W. Huang, Z. Wang, S. G. Freire, X. Yu, A. T. Smith, E. Y. Huang, H. Nguon, L. Sun, *Nat. Commun.* **2016**, *7*, 11802.

[18] Y. Wang, W. Niu, C. Y. Lo, Y. Zhao, X. He, G. Zhang, S. Wu, B. Ju, S. Zhang, *Adv. Funct. Mater.* **2020**, *30*, 2000356.

[19] K. Zhao, X. Cao, Y. Alsaid, J. Cheng, Y. Wang, Y. Zhao, X. He, S. Zhang, W. Niu, *Chem. Eng. J.* **2021**, *426*, 130870.

[20] W. Niu, X. Cao, Y. Wang, B. Yao, Y. Zhao, J. Cheng, S. Wu, S. Zhang, X. He, *Adv. Funct. Mater.* **2021**, *31*, 2009017.

[21] Q. Guo, B. Huang, C. Lu, T. Zhou, G. Su, L. Jia, X. Zhang, *Mater. Horiz.* **2019**, *6*, 996.

[22] X. Wen, S. Sun, P. Wu, *Mater. Horiz.* **2020**, *7*, 2150.

[23] L. Zheng, M. Zhu, B. Wu, Z. Li, S. Sun, P. Wu, *Sci. Adv.* **2021**, *7*, eabg4041.

[24] H. Zhou, J. Lai, X. Jin, H. Liu, X. Li, W. Chen, A. Ma, X. Zhou, *Chem. Eng. J.* **2021**, *413*, 127544.

[25] L. Fang, J. Zhang, W. Wang, Y. Zhang, F. Chen, J. Zhou, F. Chen, R. Li, X. Zhou, Z. Xie, *ACS Appl. Mater. Interfaces* **2020**, *12*, 56393.

[26] L. Fang, Z. Cai, Z. Ding, T. Chen, J. Zhang, F. Chen, J. Shen, F. Chen, R. Li, X. Zhou, Z. Xie, *ACS Appl. Mater. Interfaces* **2019**, *11*, 21895.

[27] Y. Chang, L. Wang, R. Li, Z. Zhang, Q. Wang, J. Yang, C. F. Guo, T. Pan, *Adv. Mater.* **2021**, *33*, 2003464.

[28] P. Zhu, H. Du, X. Hou, P. Lu, L. Wang, J. Huang, N. Bai, Z. Wu, N. X. Fang, C. F. Guo, *Nat. Commun.* **2021**, *12*, 4731.

[29] Y. Wan, Z. Qiu, J. Huang, J. Yang, Q. Wang, P. Lu, J. Yang, J. Zhang, S. Huang, Z. Wu, C. F. Guo, *Small* **2018**, *14*, 1801657.

[30] Y. Wang, S. Sun, P. Wu, *Adv. Funct. Mater.* **2021**, *31*, 2101494.

[31] Y. Wang, L. R. Shang, G. P. Chen, L. Y. Sun, X. X. Zhang, Y. J. Zhao, *Sci. Adv.* **2020**, *6*, aax8258.

[32] Q. Zhu, K. Van Vliet, N. Holten-Andersen, A. Miserez, *Adv. Funct. Mater.* **2019**, *29*, 1808191.

[33] W. Lu, S. Wei, H. Shi, X. Le, G. Yin, T. Chen, *Aggregate* **2021**, *2*, e37.

[34] H. J. Li, H. Zheng, Y. J. Tan, S. B. Tor, K. Zhou, *ACS Appl. Mater. Interfaces* **2021**, *13*, 12814.

[35] Y. Wang, Y. Yu, J. Guo, Z. Zhang, X. Zhang, Y. Zhao, *Adv. Funct. Mater.* **2020**, *30*, 2000151.

[36] C. Wang, P. Zhang, W. Xiao, J. Zhao, M. Shi, H. Wei, Z. Deng, B. Guo, Z. Zheng, Y. Yu, *Nat. Commun.* **2020**, *11*, 4694.

[37] E. M. Leung, M. C. Escobar, G. T. Stiubianu, S. R. Jim, A. L. Vyatskikh, Z. J. Feng, N. Garner, P. Patel, K. L. Naughton, M. Follador, E. Karshalev, M. D. Trexler, A. A. Gorodetsky, *Nat. Commun.* **2019**, *10*, 1947.

[38] Z. Mao, S. Zeng, K. Shen, A. P. Chooi, A. T. Smith, M. D. Jones, Y. Zhou, X. Liu, L. Sun, *Adv. Opt. Mater.* **2020**, *8*, 2001472.

[39] M. Gao, H. Wu, R. Plamthottam, Z. Xie, Y. Liu, J. Hu, S. Wu, L. Wu, X. He, Q. Pei, *Matter* **2021**, *4*, 1962.

[40] H. He, S. Averick, P. Mandal, H. Ding, S. Li, J. Gelb, N. Kotwal, A. Merkle, S. Litster, K. Matyjaszewski, *Adv. Sci.* **2015**, *2*, 1500069.

[41] Y. Nonomura, S. Chida, E. Seino, H. Mayama, *Langmuir* **2012**, *28*, 3799.

[42] M. L. Sauleda, H. C. W. Chu, R. D. Tilton, S. Garoff, *Langmuir* **2021**, *37*, 3309.

[43] S. Wei, H. Qiu, H. Shi, W. Lu, H. Liu, H. Yan, D. Zhang, J. Zhang, P. Theato, Y. Wei, T. Chen, *ACS Nano* **2021**, *15*, 10415.

[44] J. He, P. Xiao, J. Shi, Y. Liang, W. Lu, Y. Chen, W. Wang, P. Théato, S. W. Kuo, T. Chen, *Chem. Mater.* **2018**, *30*, 4343.

[45] H. Yuk, T. Zhang, G. A. Parada, X. Liu, X. Zhao, *Nat. Commun.* **2016**, *7*, 12028.

[46] H. Yuk, C. E. Varela, C. S. Nabzdyk, X. Mao, R. F. Padera, E. T. Roche, X. Zhao, *Nature* **2019**, *575*, 169.

[47] H. Qiu, S. Wei, H. Liu, B. Zhan, H. Yan, W. Lu, J. Zhang, S. Wu, T. Chen, *Adv. Intell. Syst.* **2021**, *3*, 2000239.

[48] Z. Jiang, M. L. Tan, M. Taheri, Q. Yan, T. Tsuzuki, M. G. Gardiner, B. Diggle, L. A. Connal, *Angew. Chem., Int. Ed.* **2020**, *59*, 7049.

[49] X. Zhou, Y. Guo, F. Zhao, W. Shi, G. Yu, *Adv. Funct. Mater.* **2020**, *32*, 2007012.

[50] J. Jia, J. H. Pu, J. H. Liu, X. Zhao, K. Ke, R. Y. Bao, Z. Y. Liu, M. B. Yang, W. Yang, *Mater. Horiz.* **2020**, *7*, 2450.

[51] H. Li, Y. Liang, G. Gao, S. Wei, Y. Jian, X. Le, W. Lu, Q. Liu, J. Zhang, T. Chen, *Chem. Eng. J.* **2021**, *415*, 128988.

[52] Y. Liang, P. Xiao, F. Ni, L. Zhang, T. Zhang, S. Wang, W. Zhou, W. Lu, S. W. Kuo, T. Chen, *Nano Energy* **2021**, *81*, 105617.

[53] H. Shi, S. Wu, M. Si, S. Wei, G. Lin, H. Liu, W. Xie, W. Lu, T. Chen, *Adv. Mater.* **2021**, 2107452.